Three-dimensional modeling of strain localization in Cosserat continuum theory

A.R. Khoei, S. Yadegari and M. Anahid

Center of Excellence in Structures and Earthquake Engineering, Department of Civil Engineering, Sharif University of Technology, P.O. Box. 11365-9313, Tehran, Iran

Abstract. *In this paper, a higher order continuum model is presented based on the Cosserat continuum theory in 3D numerical simulation of shear band localization. As the classical continuum models suffer from the pathological mesh-dependence in strain softening models, the governing equations are regularized by adding the rotational degrees-of-freedom to conventional degrees-of-freedom. The fundamental relations in three-dimensional Cosserat continuum are presented and the internal length parameters are introduced in the elasto-plastic constitutive matrix to control the shear bandwidth. Finally, the efficiency of proposed model and computational algorithm is demonstrated by a 3D strip in tensile. A comparison is performed between the classical and Cosserat theories and the effect of internal length parameter is demonstrated. Clearly, a finite shear bandwidth is achieved and the load-displacement curves are uniformly converged upon different mesh sizes.*

Keywords: *Localization, Displacement discontinuity, Cosserat theory, 3D FEM, Return mapping algorithm.*

1. INTRODUCTION

Localization of deformation refers to the emergence of narrow regions in a structure where all further deformation tends to localize, in spite of the fact that the external actions continue to follow a monotonic loading program. The remaining parts of the structure usually unload and behave in an almost rigid manner. Indeed such localization is almost certain to occur if strain softening or non-associated behavior exists, though it can be triggered even when ideal plasticity is assumed. The phenomenon has a detrimental effect on the integrity of the structure and often acts as a direct precursor to structural failure. It is observed for a wide range of materials, including rocks, concrete, soils, metals, alloys and polymers, although the scale of localization phenomena in the various materials may differ by some orders of magnitude: the band width is typically less than a millimeter in metals and several meters for crystal faults in rocks.

From a mechanical point of view the driving forces behind localization phenomena are material instabilities, that is, the constitutive relationship violates the stability criterion that the inner product of the stress rate and the strain rate is positive. Obviously, this inner product becomes negative when, in a uniaxial tension or compression test, the slope of the homogenized axial stress - axial strain curve is negative. We call this phenomenon 'strain softening'. By using the terminology 'homogenized' we refer to the fact that initial flaws and boundary conditions necessarily induce a non-homogeneous stress state in a specimen during testing. In particular, during progressive failure of the specimen these flaws and local stress concentrations will cause strongly inhomogeneous deformations of the specimen. The procedure that is normally utilized to derive stress-strain

relations, namely dividing the force by the virgin load-carrying area and dividing the displacement of the end of the specimen by the original length so as to obtain stress and strain respectively then no longer reflects what happens at a micro-level and loses physical significance.

In many physical phenomena, whose behavior is described by differential equations in a well posed manner, abrupt discontinuities in the main solution variables may develop. Such phenomena are frequently noted in solid mechanics where plastic failure or fracture can localize in surfaces on which discontinuities of stresses and displacements occur. This phenomenon was observed as early as 1972 in an early work describing a general approach to finite element solution of plasticity problems by Nayak and Zienkiewicz [1]. They experienced that even with a very coarse finite element discretization, quite narrow plastic zones occur under a punch when plastic softening is assumed. On the contrary, when the material is hardening the plasticity zone extends practically throughout the whole domain. Though not noted at the time, it became clear some years later, that material softening of the general form assumed by Nayak and Zienkiewicz, will always lead to localization with an abrupt discontinuity.

Analysis of strain localization has been an important subject in the attempt to improve the numerical simulation of structure failures. The presence of strain-softening in the constitutive laws brings great difficulties to classical (local) continuum theories [2–4]. Although it is possible to include discontinuities in the analysis (by use of special finite elements) this is complex as the position of such discontinuities has to be assumed a priori. Early efforts were devoted to obtaining failure surfaces and their associated safety factors. Later, finite element techniques allowed a more precise analysis of the stress and strain fields, using more sophisticated material models. However, the problem is no longer mathematically well posed after the onset of localization in strain-softening materials, because local continuum allows for an infinitely small band width in shear or in front of a crack tip [5]. At the numerical level, these difficulties translate in mesh dependence of solutions.

Various techniques have been implemented to provide a physically acceptable solution. Some impose restrictions on the constitutive moduli in the post-localization regime, while others artificially restrict the size of finite element by comparison to the localization zone. The former is based on enriching the continuum with non-conventional constitutive relations in such way that an internal or characteristic length scale is introduced. Bifurcation analysis techniques based on the early work of Thomas [6] and Rice [7] were adopted by many researchers to determine the shear band localization (de Borst [8], Runneson et al. [9], Pijaudier-Cabot and Benallal [10] and Simo et al [11]). Non-local theories are the Cosserat continuum [12, 13], the higher gradient theories (Triantafyllidis and Ainfantis [14]), and the integral theory or the gradient theory (de Borst and Mulhlaus [15] and Muhlhaus and Ainfantis [16]). The later is based on a mesh refinement technique using the normal, continuous, approximations to all the variables (Pastor et al. [17], Belytschko and Tabbara [18], Zienkiewicz et al. [19], Lewis and Khoei [20] and Khoei and Lewis [21]). The aim of this research is to capture the localization phenomena by restriction on the material property matrix in the post-localization regime based on the Cosserat continuum theory.

The Cosserat continuum theory, first proposed by Cosserat brothers in 1909 [22], has attracted many attentions in last two decades. The first implementation of the theory into a finite element code was made by de Borst [23] and de Borst and his co-workers [13, 15, 24]. This theory has two main characteristics. Firstly, the rotational degree-of-freedom is taken into account in addition to translation degrees-of-freedom. In fact, the introduction of rotational degree-of-freedom leads to the existence of moment stresses (moment per area) in addition to the stresses of classic continuum. Secondly, the internal length scales is introduced in the field of constitutive equation. This parameter, which plays the most important role in controlling shear bandwidth, relates couple stresses to micro-curvature. Tejchman and Wu [25] proposed the Cosserat continuum model as the regularization approach to analyze strain localization problems. An application of adaptive strategy was presented by Peric et al. [26] in numerical simulation of strain localization using Cosserat continua. Iordache and Willam [27] proposed the micropolar Cosserat continua to examine the regularization properties of discontinuous bifurcation problems. The Cosserat theory was applied to the localization behavior of associated and non-associated materials by Carmer et al. [28].

The Cosserat theory was implemented not only to predict the phenomena of localization, but also to simulate the variety of other problems ranging from the mechanics of rocks to powder forming processes. A microstructure plastic continuum was developed by Chambon et al. [29] based on the local second gradient theory in strain localization of geomaterials. The theory was proposed by Forest et al. [30] to study the localization patterns at a crack tip in generalized single crystal plasticity. Sulem and Cerrolaza [31] applied the Cosserat theory to study the scale effect in measuring of strength parameters of rocks in indentation test. A study of localized deformation pattern in granular media was performed by Nubel and Huang [32]. A pressure-dependent elasto-plastic Cosserat continuum was presented by Li and Tang [33] in modeling strain localization using a consistent return mapping algorithm. A finite strain elasto-plasticity Cosserat formulation was presented by Neff [34] based on the multiplicative decomposition of deformation gradient, following the earlier work of Sievert et al. [35]. The Cosserat continuum theory was employed by Mori [36] to powder forming processes due to microscopic rotations of powder particles.

The main objective of present paper is to extend the 2D Cosserat theory presented by Khoei et al. [37, 38] for strain softening plasticity to three-dimensional modeling of shear band localization. A numerical solution is developed based on the higher order continuum model in prediction of localization phenomena. The fundamental relations in Cosserat continuum are presented for 3D solid problems. The governing equations are regularized by adding the rotational degrees-of-freedom to conventional degrees-of-freedom and an internal length scale in the field of constitutive equation. Generally, due to path dependency of the solution in nonlinear analysis, the loading is applied in an incremental manner with an iterative linearization, using the Newton-Raphson method in each increment.

2. COSSERAT CONTINUUM THEORY

In Cosserat theory, the independent rotation vector (micro-rotation) is contributed

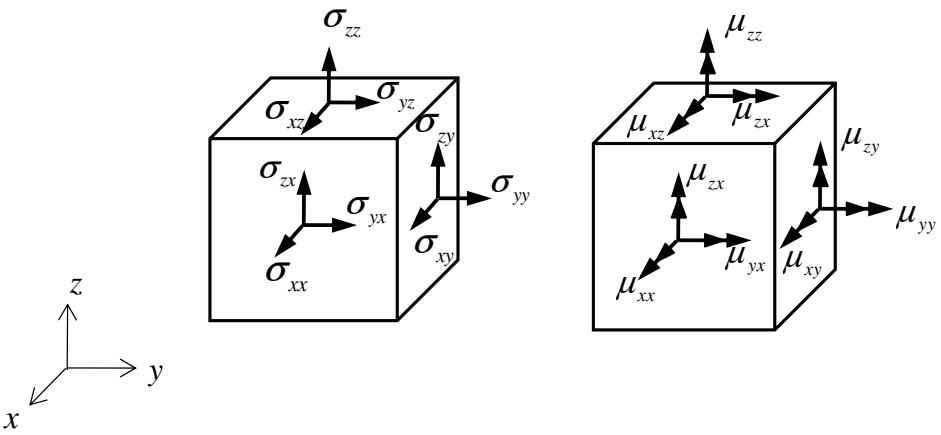

Figure 1.The stress and couple-stress components in three dimensional space

through the governing equations, which is distinct from the macro-rotation introduced by the gradient of displacement vector. These micro-rotations are included as a part of degree of freedom for a point aside of displacement vector . Thus, the strain components in Cosserat continuum can be defined as

$$\begin{aligned} \varepsilon_{ij} &= u_{i,j} + e_{ijk}\varphi_k \\ \kappa_{ij} &= \varphi_{i,j} \end{aligned} \tag{1}$$

where e_{ijk} is the permutation symbol. Due to contribution of micro-rotations, the Cosserat strain tensor is no longer symmetric. However, the substitution of micro-rotations with macro-rotations results in symmetry tensor which is not the subject of this study. In above relation, κ_{ij} is the torsion-curvature, called wryness tensor, and is conjugated to the couple stress tensor μ_{ij} . In Figure 1, two different types of couple-stresses are presented which can be interpreted as torsion and bending couples acting on the surface. These two couple stresses have different characteristic lengths which can be related to the curvature tensor through the elasticity tensor.

In Cosserat theory, it is assumed that the interaction between two particles of the body occurs through the means of traction vector $t_i ds$ and the means of moment vector $m_i ds$. The surface forces and couples can be then expressed as follows

$$t_i = \sigma_{ij} n_j \quad , \quad m_i = \mu_{ij} n_j \tag{2}$$

Applying the Green's theorem with respect to body forces and body couples, the equilibrium governing equations in Cosserat continuum can be written as [39]

$$\begin{aligned} \sigma_{ij,j} + f_i &= \rho \ddot{u}_i \\ \mu_{ij,j} - e_{ikl}\sigma_{kl} + c_i &= I\ddot{\varphi}_i \end{aligned} \tag{3}$$

where f_i and c_i denote the body force and body couple, respectively, and ρ and I indicate the mass density and rotational inertia. The second equilibrium equation presents the moment of momentum, and due to this equation the symmetry of stress tensor is no longer available, i.e. $\sigma_{ij} \neq \sigma_{ji}$, that can be complied with its conjugate in strain space ε_{ij} .

2.1. Three-Dimensional Cosserat Elasticity

In order to obtain an appropriate elastic modulus for isotropic Cosserat medium, two

assumptions need to be taken into account. First, consider that the stress and couple-stress components do not interact together so we will have two distinct equations, each of them dealing with either stresses or couple-stresses. In this case, the governing equation for stress components is slightly different from the classical continuum because of lack symmetry in stress tensor, as mentioned earlier. Thus, the fourth order tensor that relates the stress to strain tensor has three constants, one more than its relevant classical theory, in which this additional parameter is called G_c . Secondly, in order to relate the couple-stresses to curvatures we assume no interaction between bending and torsion couple stresses in constitutive equation, thus the number of independent constants can be reduced to two parameters.

Combining the stress and couple-stress vectors $\boldsymbol{\sigma}=[\tilde{\boldsymbol{\sigma}}, \boldsymbol{\mu}]^{\mathrm{T}}$ to a single generalized vector , with $\tilde{\boldsymbol{\sigma}}$ and μ denoting by

$$\tilde{\boldsymbol{\sigma}}=[\sigma_{xx}, \sigma_{yy}, \sigma_{zz}, \sigma_{xy}, \sigma_{yx}, \sigma_{yz}, \sigma_{zy}, \sigma_{xz}, \sigma_{zx}]^{\mathrm{T}}$$
$$\boldsymbol{\mu}=[\mu_{xx}, \mu_{yy}, \mu_{zz}, \mu_{xy}, \mu_{yx}, \mu_{yz}, \mu_{zy}, \mu_{xz}, \mu_{zx}]^{\mathrm{T}} \quad (4)$$

And combining the strain and curvature vectors to a single generalized strain vector as $\boldsymbol{\varepsilon}=[\tilde{\boldsymbol{\varepsilon}}, \boldsymbol{\kappa}]^{\mathrm{T}}$, where $\tilde{\boldsymbol{\varepsilon}}$ and κ are

$$\tilde{\boldsymbol{\varepsilon}}=[\varepsilon_{xx}, \varepsilon_{yy}, \varepsilon_{zz}, \varepsilon_{xy}, \varepsilon_{yx}, \varepsilon_{yz}, \varepsilon_{zy}, \varepsilon_{xz}, \varepsilon_{zx}]^{\mathrm{T}}$$
$$\boldsymbol{\kappa}=[\kappa_{xx}, \kappa_{yy}, \kappa_{zz}, \kappa_{xy}, \kappa_{yx}, \kappa_{yz}, \kappa_{zy}, \kappa_{xz}, \kappa_{zx}]^{\mathrm{T}} \quad (5)$$

Hence, the constitutive relation for an elastic Cosserat medium can be defined as $\sigma=\mathrm{D}^e\varepsilon$, where D^e is the linear elastic operator defined as

$$\mathbf{D}^e=\mathrm{diag}[\mathbf{D}_1, \mathbf{D}_2, \mathbf{D}_2, \mathbf{D}_2, \mathbf{D}_3] \quad (6)$$

where

$$\mathbf{D}_1=\begin{bmatrix} 2Gc_1 & 2Gc_2 & 2Gc_2 \\ 2Gc_2 & 2Gc_1 & 2Gc_2 \\ 2Gc_2 & 2Gc_2 & 2Gc_1 \end{bmatrix},\ c_1=\frac{1-\nu}{1-2\nu},\ c_2=\frac{\nu}{1-2\nu}$$
$$\mathbf{D}_2=\begin{bmatrix} G+G_c & G-G_c \\ G-G_c & G+G_c \end{bmatrix}$$
$$\mathbf{D}_3=\mathrm{diag}\left[2G\ell_t^2, 2G\ell_t^2, 2G\ell_t^2, 2G\ell_b^2, 2G\ell_b^2, 2G\ell_b^2, 2G\ell_b^2, 2G\ell_b^2, 2G\ell_b^2\right] \quad (7)$$

where ℓ denotes the internal length parameter for both torsion and bending couple-stresses, which indicates physically the width of shear bands in localized region. ℓ_t can be determined by the torsion of a circular cylindrical rod, and the bending of a circular cylindrical rod can be used for determination of ℓ_b . Taking the internal length parameters into the curvature vector (5) to make all components dimensionless, the new forms of μ and κ can be rewritten as

$$\boldsymbol{\mu}=[\mu_{xx}/\ell_t, \mu_{yy}/\ell_t, \mu_{zz}/\ell_t, \mu_{xy}/\ell_b, \mu_{yx}/\ell_b, \mu_{yz}/\ell_b, \mu_{zy}/\ell_b, \mu_{xz}/\ell_b, \mu_{zx}/\ell_b]^{\mathrm{T}}$$
$$\boldsymbol{\kappa}=[\kappa_{xx}\ell_t, \kappa_{yy}\ell_t, \kappa_{zz}\ell_t, \kappa_{xy}\ell_b, \kappa_{yx}\ell_b, \kappa_{yz}\ell_b, \kappa_{zy}\ell_b, \kappa_{xz}\ell_b, \kappa_{zx}\ell_b]^{\mathrm{T}} \quad (8)$$

2.2. Three-Dimensional Cosserat Elasto-plasticity

In order to introduce the internal length scale into the set of constitutive equations, the classical model of pressure-independent J_2-elasto-plasticity is generalized by introducing additional degrees of freedom within the Cosserat continuum. Hence, an extension of classical J_2-flow theory in Cosserat continuum is defined as [24]

$$J_2=a_1 s_{ij}s_{ij}+a_2 s_{ij}s_{ji}+\frac{1}{\ell^2}a_3\mu_{ij}\mu_{ij} \quad (9)$$

where s_{ij} is the deviatoric stress tensor, ℓ is either ℓ_t or ℓ_b, and a_1,a_2 and a_3 are the material parameters. In the absence of couple-stresses, i.e. $\mu_{ij}=0$ and $s_{ij}=s_{ji}$, equation (9) reduces to

$$J_2 = (a_1 + a_2) s_{ij} s_{ij} \tag{10}$$

in which we need to enforce $a_1+a_2=1/2$ in order to obtain the classical expression for J_2. Thus, the yield criteria can be presented in a similar manner to classical continuum as

$$F = (3J_2)^{0.5} - \bar{\sigma}(\bar{\varepsilon}^p) = 0 \tag{11}$$

where $\bar{\sigma}$ denotes the yield stress, which is a function of the effective plastic strain $\bar{\varepsilon}^p$. Equation (9) can be rewritten in a matrix format as

$$J_2 = \frac{1}{2}\boldsymbol{\sigma}^{\mathrm{T}}\mathbf{P}\boldsymbol{\sigma} \tag{12}$$

where

$$\mathbf{P} = \mathrm{diag}\,[\mathbf{P}_1,\ \mathbf{P}_2,\ \mathbf{P}_2,\ \mathbf{P}_2,\ \mathbf{P}_3] \tag{13}$$

where

$$\mathbf{P}_1 = \begin{bmatrix} 2/3 & -1/3 & -1/3 \\ -1/3 & 2/3 & -1/3 \\ -1/3 & -1/3 & 2/3 \end{bmatrix}$$

$$\mathbf{P}_2 = \begin{bmatrix} a_1 & a_2 \\ a_2 & a_1 \end{bmatrix}$$

$$\mathbf{P}_3 = \mathrm{diag}\left[2a_3,\ 2a_3,\ 2a_3,\ 2a_3,\ 2a_3,\ 2a_3,\ 2a_3,\ 2a_3,\ 2a_3\right] \tag{14}$$

As in classical plasticity, the plastic strain is related to yield criteria as follow

$$\dot{\boldsymbol{\varepsilon}}^p = \dot{\lambda}\frac{\partial F}{\partial \boldsymbol{\sigma}} = \frac{3\dot{\lambda}}{2\bar{\sigma}(\bar{\varepsilon}^p)}\mathbf{P}\boldsymbol{\sigma} \tag{15}$$

where λ is the plastic multiplier. The effective plastic strain, defined in equation (15), can be evaluated by

$$\bar{\varepsilon}^p = \left(\frac{2}{3}(\boldsymbol{\varepsilon}^p)^{\mathrm{T}}\,\mathbf{P}\,\boldsymbol{\varepsilon}^p\right)^{0.5} \tag{16}$$

3. COMPUTATIONAL ALGORITHM

The algorithm presented here is completely similar to classical continuum algorithm when the von-Mises yield criterion is adopted. In what follows, we first present the return mapping algorithm to obtain the plastic multiplier $\Delta\lambda$ at each increment, the consistent tangent matrix is then extracted to achieve the quadratic convergency rate in Newton-Raphson algorithm.

3.1. Return Mapping Algorithm

The trial stress at the beginning of the new step can be calculated as

$$\boldsymbol{\sigma}_t = \boldsymbol{\sigma}_0 + \mathbf{D}^e\Delta\boldsymbol{\varepsilon} \tag{17}$$

In the above equation it is assumed that the stress increment is related to strain increment through the elastic material property matrix. The new stress state at the end of the increment is the sum of the stress at the beginning of the step and the stress increment, i.e.

$$\boldsymbol{\sigma}_p = \boldsymbol{\sigma}_0 + \Delta\boldsymbol{\sigma} \tag{18}$$

Substituting equations (15) and (17) into equation (18), we obtain the following explicit expression

$$\boldsymbol{\sigma}_p = \left(\mathbf{I} + \frac{3G\,\Delta\lambda}{\bar{\sigma}(\bar{\varepsilon}^p)}\mathbf{P}\right)^{-1}\boldsymbol{\sigma}_t \tag{19}$$

in which the only unknown parameter is $\Delta\lambda$. If plasticity occurs (i.e., $F(\boldsymbol{\sigma}_t, \bar{\varepsilon}_0^p) > 0$), a correction for plastic flow must be applied. To this end the yield condition $F(\boldsymbol{\sigma}_n, \bar{\varepsilon}_n^p) = 0$, where the subscript *n* denotes the value of a quantity after correction for plastic flow, is developed in a truncated Taylor series around $(\boldsymbol{\sigma}_t, \bar{\varepsilon}_0^p)$ as [23]

$$F(\boldsymbol{\sigma}_t,\ \bar{\varepsilon}_0^p) = \Delta\lambda\left(H + \frac{\partial F}{\partial \boldsymbol{\sigma}}^{\mathrm{T}}\ \mathbf{D}^e\ \frac{\partial F}{\partial \boldsymbol{\sigma}} \right) \tag{20}$$

where H is the hardening parameter and can be defined similar to that of the classic continuum as $H = \partial\bar{\sigma}/\partial\bar{\varepsilon}_0^p$. Substituting $\partial F/\partial\sigma$ from equation (15) into equation (20), we obtain an explicit expression for the plastic multiplier $\Delta\lambda$ as

$$\Delta\lambda = \frac{F(\boldsymbol{\sigma}_t,\ \bar{\varepsilon}_0^p)}{H + 3G} \tag{21}$$

With expression (21) for the magnitude of the plastic strain increment, the computation for elasto-plasticity in Cosserat continuum is completed in analogy to a conventional plasticity model. The plastic strain increment in each step can be determined from equations (15) and (21) and then, the corrected value of stress can be obtained from equations (17) and (19). For numerical calculations the coefficients of P are chosen as $a_1 = a_2 = 1/4$ and $a_3 = 1/2$ [24].

3.2. Consistent Tangent Modulus

In order to achieve the full advantage of quadratic convergence rate in Newton's algorithm, the consistent tangent modulus needs to be introduced for Cosserat continuum model. The stress update can be computed in standard elasto-plasticity by an integral along a given path from the initial state to the final state as follows

$$\boldsymbol{\sigma} = \boldsymbol{\sigma}_0 + \int_{\boldsymbol{\varepsilon}_0}^{\boldsymbol{\varepsilon}} \mathbf{D}^{ep} d\boldsymbol{\varepsilon} \tag{22}$$

where the elasto-plastic tangent modulus is defined as

$$\mathbf{D}^{ep} = \left(\frac{\partial \boldsymbol{\sigma}}{\partial \boldsymbol{\varepsilon}} \right)_{\boldsymbol{\varepsilon}} \tag{23}$$

Algorithmically, the stress update is calculated as

$$\boldsymbol{\sigma}_i = \boldsymbol{\sigma}_0 + \mathbf{S}(\boldsymbol{\varepsilon}_0,\ \Delta\boldsymbol{\varepsilon}_i) \tag{24}$$

where S is a nonlinear mapping operator depends on the numerical method of plastic strain integration within the increment $\Delta\varepsilon_i$ defined as

$$\Delta\boldsymbol{\varepsilon}_i = \sum_{j=1}^{i} d\boldsymbol{\varepsilon}_j \tag{25}$$

The consistent (algorithmic) tangent modulus is defined as [40]

$$\mathbf{D}^{ep}_{\mathrm{cons}}(\boldsymbol{\varepsilon}_0, \Delta\boldsymbol{\varepsilon}_i) = \left(\frac{\partial \boldsymbol{\sigma}_i}{\partial \boldsymbol{\varepsilon}} \right)_{\boldsymbol{\varepsilon}_0, \Delta\boldsymbol{\varepsilon}_i} = \left(\frac{\partial \mathbf{S}}{\partial \Delta\boldsymbol{\varepsilon}} \right)_{\boldsymbol{\varepsilon}_0, \Delta\boldsymbol{\varepsilon}_i} \tag{26}$$

in which it is in general non-symmetric and for finite, large steps differs significantly from D^{ep}. An explicit definition of $D^{ep}{}_{cons}$ for associated J_2 flow plasticity can be obtained by differentiating from equation (19) as

$$\dot{\boldsymbol{\sigma}} = \hat{\mathbf{D}}^e \left(\dot{\boldsymbol{\varepsilon}} - \dot{\lambda} \frac{\partial F}{\partial \boldsymbol{\sigma}} \right) \tag{27}$$

where

$$\left[\hat{\mathbf{D}}^e \right]^{-1} = \left[\mathbf{D}^e \right]^{-1} + \Delta\lambda \sqrt{\frac{3}{2}} \frac{\boldsymbol{\sigma}^{\mathrm{T}}\mathbf{P}\,\boldsymbol{\sigma}\,\mathbf{P} - \mathbf{P}\,\boldsymbol{\sigma}\,\boldsymbol{\sigma}^{\mathrm{T}}\mathbf{P}}{\left(\boldsymbol{\sigma}^{\mathrm{T}}\mathbf{P}\,\boldsymbol{\sigma} \right)^{3/2}} \tag{28}$$

where $\hat{\mathbf{D}}^e$ is the so-called pseudo-elastic stiffness operator. Following the standard procedure for derivation of D^{ep}, which employs the consistency condition $F(\boldsymbol{\sigma},\ \bar{\varepsilon}^p) = 0$, the consistent tangent modulus $D^{ep}{}_{cons}$ can be extracted as

$$\mathbf{D}^{ep}_{\mathrm{cons}} = \hat{\mathbf{D}}^e - \frac{\hat{\mathbf{D}}^e \mathbf{n}\mathbf{n}^{\mathrm{T}} \hat{\mathbf{D}}^e}{H + \mathbf{n}^{\mathrm{T}} \hat{\mathbf{D}}^e \mathbf{n}} \tag{29}$$

where $\mathbf{n} = \partial F/\partial\sigma$. From equation (28), it can be seen that when strain increment is very small (i.e., at limit $\Delta\lambda \to 0$), $D^{ep}{}_{cons}$ turns into D^{ep} .

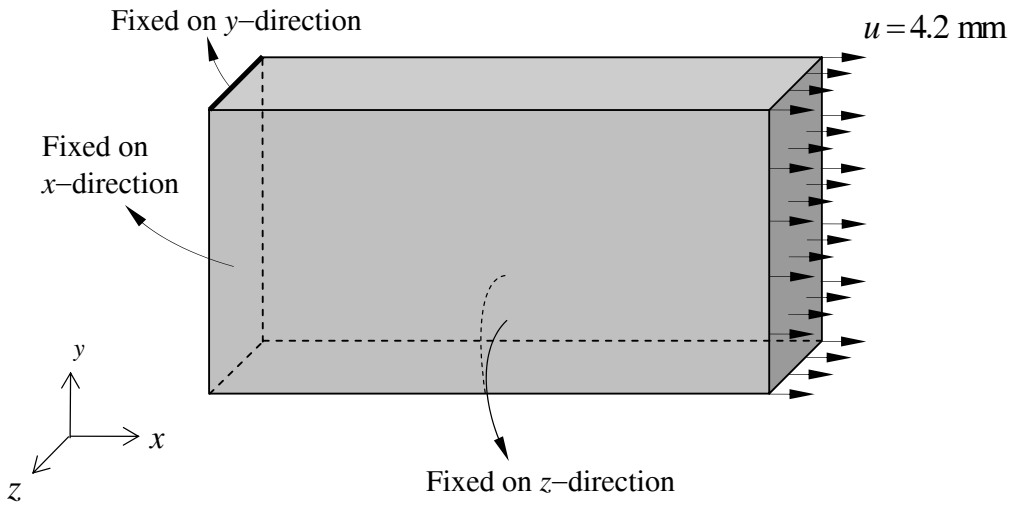

Figure 2.The geometry and boundary conditions of a 3D strip in tensile

4. NUMERICAL SIMULATION RESULTS

In order to demonstrate the effective performance of proposed computational algorithm, the implementation of Cosserat continuum model on the plastic flow in localization analysis is illustrated. The Cosserat finite element analysis is carried out for 20-noded hexahedral elements with 6 degrees-of-freedom at each node, including three rotational and three translational degrees-of-freedom. A strip in tensile with strain softening Cosserat plasticity is analyzed numerically, as shown in Figure 2. Three-dimensional numerical analysis is compared with its two-dimensional model to verify the correctness of proposed model and the capability of the algorithm in capturing shear band localization. The effect of Cosserat theory on regularization of the results is illustrated by performing a comparison with classical analysis. The effect of internal length parameters in Cosserat continuum is shown on the shear band width and corresponding load-displacement curves.

A strip with 60 mm width, 120 mm height and 22.5 mm depth is subjected to a uniform displacement in x–direction. The strip is restrained in x–direction at the left hand side and y–direction on the upper edge of fixed support. All external nodes in x–y planes are restrained in z–direction (Figure 2). The rotational degrees of freedom are free for all nodal points. The 3D numerical simulation is performed by using 20 noded-hexahedral elements. The material parameters chosen are as follows; $E=4000\ N/mm^2$, $v=0.49$, $G_c=2000\ N/mm^2$, $\sigma_Y=100\ N/mm^2$, and the plastic softening modulus $H=-120\ N/mm^2$. The internal length parameter varies from $1mm$ to $3mm$. A weak zone is assumed on the upper left edge of the plate to trigger the localization mechanism. The material parameters of soft zone are similar to strip except $\sigma_Y=98\ N/mm2$ and $v=0.30$.

In Figure 3, the deformed meshes of 3D (16x8x3) and 2D (16x8) models are shown for both the Cosserat and classical theories at $u=4.2\ mm$. The 2D and 3D Cosserat analyses are performed at different internal length

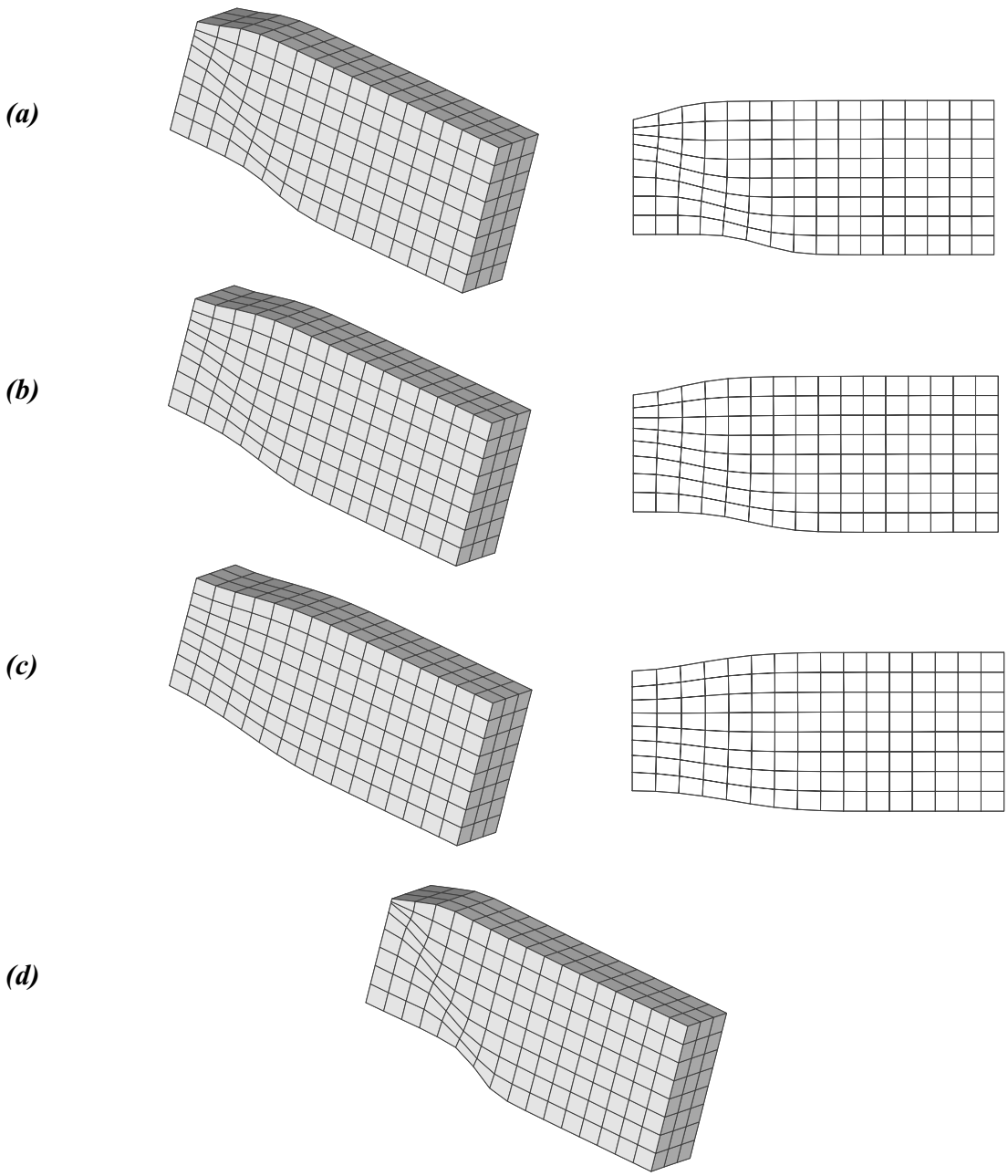

Figure 3. The deformed meshes of 3D (16×8×3) and 2D (16×8) models for a strip in tensile using Cosserat theory at $u=4.2mm$; **a)** $\ell_b=1mm$, $\ell_t=0$ **b)** $\ell_b=2mm$, $\ell_t=0$, **c)** $\ell_b=3mm$, $\ell_t=0$, **d)** The classical theory

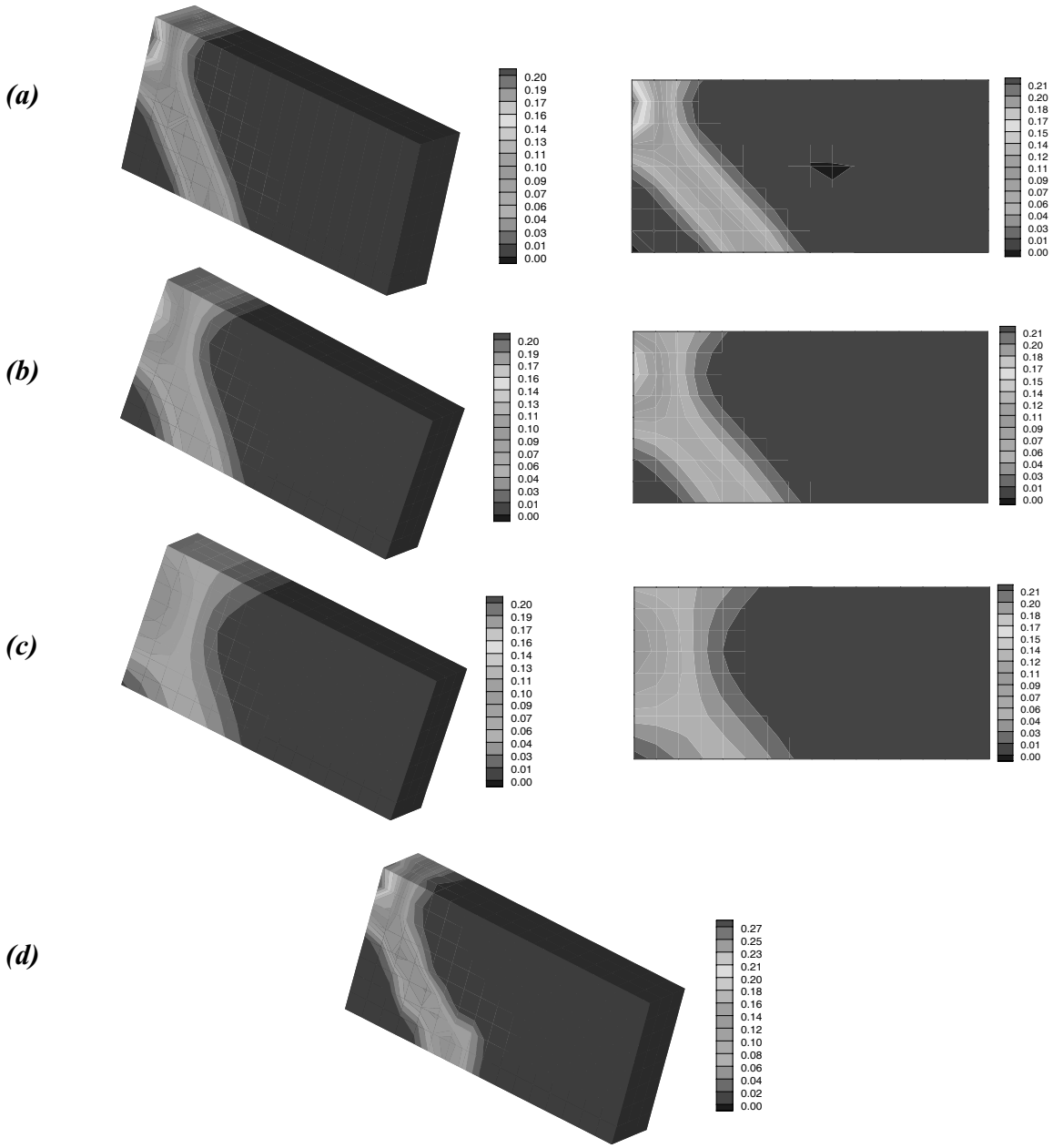

Figure 4.The effective plastic strain contours of 3D (16x8x3) and 2D (16x8) models for a strip in tensile using Cosserat theory at $u=4.2mm$; **a)** $\ell_b=1mm$, $\ell_t=0$ **b)** $\ell_b=2mm$, $\ell_t=0$, **c)** $\ell_b=3mm$, $\ell_t=0$ **d)** The classical theory

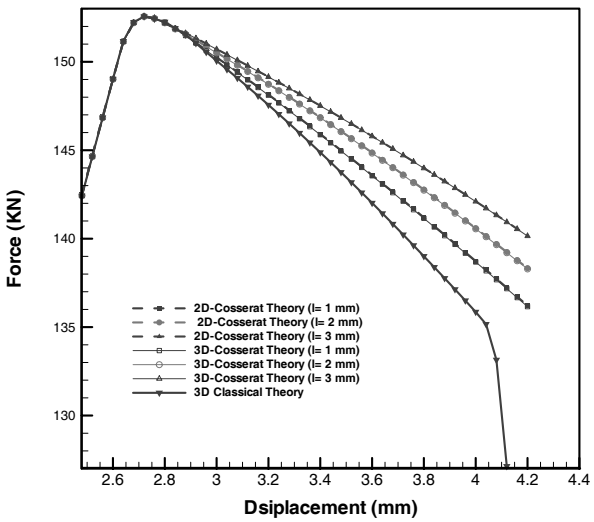

Figure 5.The load–displacement curves for a strip in tensile using 3D (16x8x3) and 2D (16x8) models; A comparison between the Cosserat and classical continuum analyses

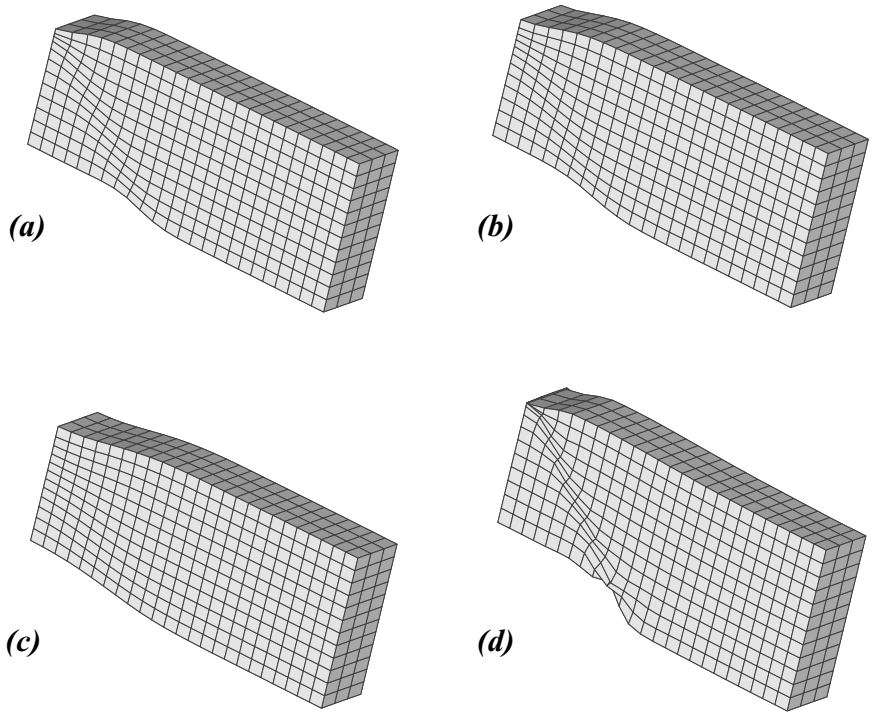

Figure 6.The deformed meshes of 3D (24x12x3) analyses for a strip in tensile using Cosserat theory at $u=4.2mm$; **a)** $\ell_b=1mm$, $\ell_t=0$ **b)** $\ell_b=2mm$, $\ell_t=0$, **c)** $\ell_b=3mm$, $\ell_t=0$ **d)** The classical theory

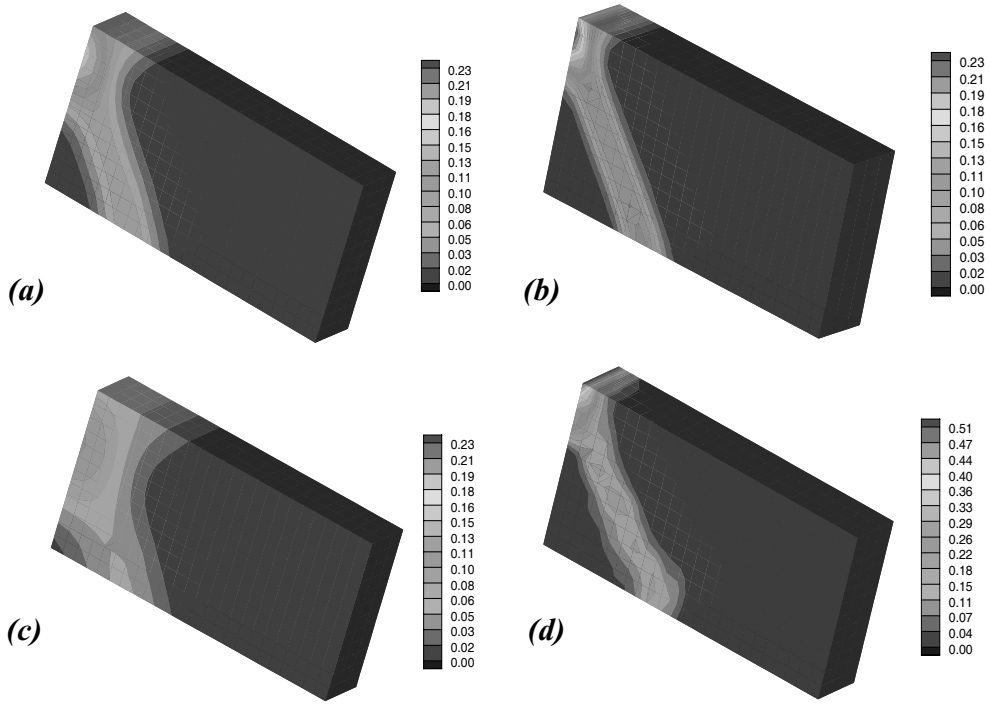

Figure 7.The effective plastic strain contours of 3D (24x12x3) analyses for a strip in tensile using Cosserat theory at $u=4.2mm$ **a)** $\ell_b=1mm$, $\ell_t=0$ **b)** $\ell_b=2mm$, $\ell_t=0$, **c)** $\ell_b=3mm$, $\ell_t=0$ **d)** The classical theory

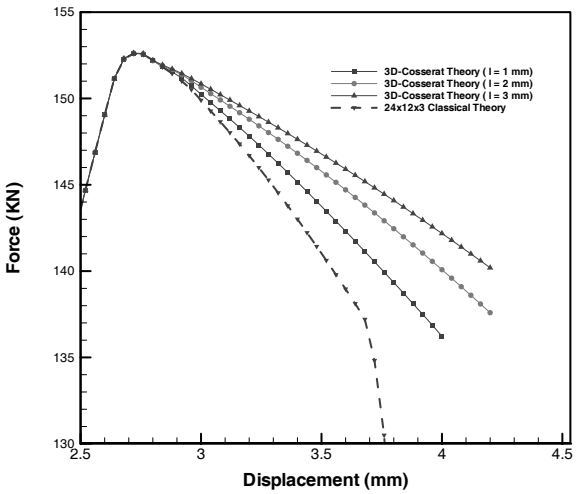

Figure 8.The load–displacement curves for a strip in tensile using 3D (24x12x3) model; A comparison between the Cosserat analysis with different internal lengths and classical theory

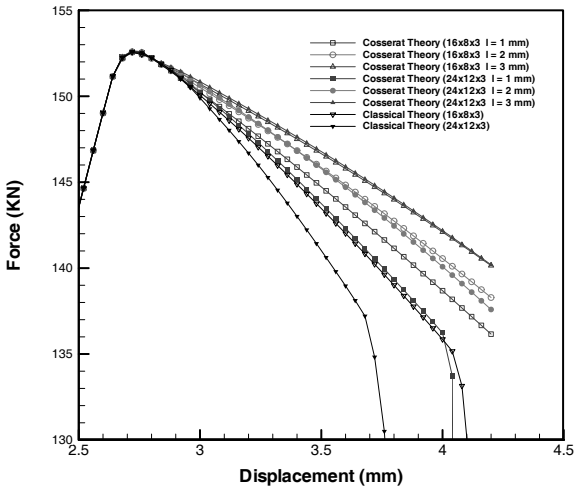

Figure 9.The load–displacement curves for a strip in tensile using 3D Cosserat analysis; A comparison between two different meshes

parameters of $\ell_b = 1,2,3$ *mm* and $\ell_t = 0$. Obviously, the Cosserat analyses regularize the localization zone while the classical solution shows a sudden jump on the edge of localized region. In Figure 4, the effective plastic strain contours are presented for both 3D and 2D models, which can be compared with classical theory. The 3D effective plastic strain contours are almost identical with those obtained from 2D simulation results. The effect of internal length parameter in Cosserat theory can be clearly observed on the shear band width. As can be seen, by increasing the internal length, the shear band width becomes wider in localized zone. In this figure, a non-smooth shear band localization is evident in the effective plastic strain contour of classical theory. The variations of predicted reaction with displacement are plotted in Figure 5 for 3D and 2D models using Cosserat theory. The 2D Cosserat results can be compared with those reported by de Borst in reference [24]. As can be seen from this figure, with reduction of internal length parameter the load-displacement curve converges to the classical solution, in which for zero value of internal length parameter the classical result has been achieved.

In order to investigate the accuracy of numerical simulation results, a mesh of 24x12x3 hexahedral elements is employed for the proposed strip problem. Figure 6 presents the deformed meshes at different internal length parameters in Cosserat theory and that obtained from classical theory. The mesh dependency is obvious in classical theory while the Cosserat theory preserves a smooth behavior in deformed shape of different internal lengths. For classical solution, the localized band width is much smaller than previous one obtained from coarse mesh (Figure 3) and the mesh distortion can be observed. In Figure 7, the effective plastic strain contours are shown for both classical and Cosserat theories. In Cosserat theory, the maximum values of effective plastic strain are similar to those obtained from coarse mesh in Figure 4, while for classical solution its maximum value is almost twice the coarse mesh. In Figure 8, the load–displacement curves are plotted for both techniques. As can be expected, by reducing the value of internal length parameter to zero the Cosserat theory converges to classical theory. In order to

demonstrate the mesh objectivity in Cosserat theory, the variations with displacement of reaction force are presented in Figure 9 for the coarse and fine meshes. Remarkable agreement can be observed between two different meshes.

5. CONCLUSION

In the present paper, the Cosserat finite element analysis was presented for the history-dependent material of elasto-plasticity with special reference to strain localization in 3D problems. The governing equations were regularized by adding rotational degrees-of-freedom to the conventional degrees-of-freedom in Cosserat continuum theory. The fundamental equations of Cosserat elasto-plasticity was presented in three-dimensional framework, including: the kinematic relation, stress-strain relationship, yield criterion, flow rule, hardening rule and consistent tangent matrix. The internal length parameters were introduced in the elasto-plastic constitutive matrix to control the shear bandwidth. The capability of computational algorithm was demonstrated through the numerical analysis of a 3D strip in tensile. The Cosserat finite element analysis was carried out for 20-noded hexahedral elements with 6 degrees-of-freedom at each node, including three rotational and three translational degrees-of-freedom. A comparison was performed between the classical and Cosserat theories and the effect of internal length parameter was demonstrated. The existence of mesh dependency and instability has been shown in classical continuum theory. Clearly, a finite shear bandwidth is achieved and the load-displacement curves are uniformly converged upon different mesh sizes.

REFERENCES

[1] Nayak GC, Zienkiewicz, OC. Elasto-plastic stress analysis, Generalization for various constitutive relations including strain softening, Int J Num Meth Eng, 1972; 5: 113-135.

[2] Bazant ZP, Belytschko TB, Chang TP. Continuum theory for strain softening. J Eng Mech Div, ASCE 1984; 110: 1666–1692.

[3] Pietruszczak S, Stolle DE. Deformation of strain softening materials, Part I: Objectivity of finite element solutions based on conventional strain softening formulations. Comput Geotech, 1985; 1: 99–115.

[4] Belytschko T, Fish J, Englemann BE. A finite element with embedded localization zones. Comput Meth Appl Mech Eng, 1988; 70: 59–89.

[5] Benallal A, Tvergaard V. Nonlocal continuum effects on bifurcation in the plane strain tension–compression test. J Mech Phys Solids, 1995; 43: 741–770.

[6] Thomas TY. Plastic Flow and Fracture in Solids. Academic Press, New York, 1961.

[7] Rice JR. The localization of plastic deformation. in: W.T. Koiter (Ed.), Theoretical and Applied Mechanics, North-Holland, Amesterdam, 1977; 207–220.

[8] De Borst R. Bifurcations in finite element models with a nonassociated flow law. Int J Numer Anal Meth Geomech, 1988; 12: 99–116.

[9] Runneson K, Ottossen NS, Peric D. Discontinuous bifurcation of elasto-

plastic solution at plane stress and plane strain. Int J Plasticity, 1991; 7: 99–121.

[10] Pijaudier-Cabot G, Benallal A. Strain localization and bifurcation in a nonlocal continuum. Int J Solids Struct, 1993; 30: 1761–1771.

[11] Simo JC, Oliver J, Armero F. An analysis of strong discontinuities induced by strain-softening in rate-independent inelastic solids. Comput Mech, 1993; 12: 227–249.

[12] Fleck NA, Hutchinson JW. A phenomenological theory of strain gradient plasticity. J Mech Phys Solids, 1993; 41: 1825–1857.

[13] De Borst R, Sluys LJ, Muhlhaus HB, Pamin J. Fundamental issues in finite element analysis of localization of deformation. Eng Comput, 1993; 10: 99–121.

[14] Triantafyllidis N, Ainfantis E. A gradient approach to localization of deformation. I: Hyperelastic materials. J Elasticity, 1986; 16: 225–237.

[15] De Borst R, Muhlhaus HB. Gradient-dependent plasticity: formulation and algorithmic aspects. Int J Num Meth Eng, 1992; 35: 521–539.

[16] Muhlhaus HB, Ainfantis E. A variational principle for gradient plasticity. Int J Solids Struct, 1991; 28: 845–857.

[17] Pastor M, Peraire J, Zienkiewicz OC. Adaptive remeshing for shear band localization problem. Arch Appl Mech, 1991; 61: 30–39.

[18] Belytschko T, Tabbara M. H-adaptive finite element methods for dynamic problems with emphasis on localization. Int J Num Meth Eng, 1993; 36: 4245–4265.

[19] Zienkiewicz OC, Huang M, Pastor M. Localization problems in plasticity using finite elements with adaptive remeshing. Int J Num Anal Meth Geomech, 1995; 19: 127–148.

[20] Lewis RW, Khoei AR. Numerical analysis of strain localization in metal powder forming processes. Int J Num Meth Eng, 2001; 52: 489–501.

[21] Khoei AR, Lewis RW. H-adaptive finite element analysis for localization phenomena with reference to metal powder forming. Finite Elem Anal Des, 2002; 38: 503–519.

[22] Cosserat E, Cosserat F. Theorie des Corps Deformable. Hermann, Paris, 1909.

[23] De Borst R. Simulation of strain localization: a reappraisal of Cosserat continuum. Eng Comput 1991; 8: 317–332.

[24] De Borst R. A generalization of J2-flow theory for polar continua. Comput Meth Appl Mech Eng, 1993; 103: 347–362.

[25] Tejchman J, Wu W. Numerical study on patterning of shear bands in Cosserat continuum. Acta Mech, 1993; 99: 61–74.

[26] Peric D, Yu J, Owen DRJ. On error estimates and adaptivity in elastoplastic solids: applications to the

numerical simulation of strain localization in classical and Cosserat continua. Int J Num Meth Eng, 1994; 37: 1351–1379.

[27] Iordache MM, Willam K. Localized failure analysis in elastoplastic Cosserat continua. Comput Meth Appl Mech Eng, 1998; 151: 559–586.

[28] Cramer H, Findeiss R, Steinl G, Wunderlich W. An approach to the adaptive finite element analysis in associated and non-associated plasticity considering localization phenomena. Comput Meth Appl Mech Eng, 1999; 176: 187–202.

[29] Chambon R, Caillerie D, Matsuchima T. Plastic continuum with microstructure, local second gradient theories for geomaterials: localization studies. Int J Solids Struct, 2001; 38: 8503–8527.

[30] Forest S, Boubidi P, Sievert R. Strain localization patterns at a crack tip in generalized single crystal plasticity. Scripta Mater. 2001; 44: 953–958.

[31] Sulem J, Cerrolaza M. Finite element analysis of the indentation test on rocks with microstructure. Comput Geotech, 2002; 29: 95–117.

[32] Nubel K, Huang W. A study of localized deformation pattern in granular media. Comput Meth Appl Mech Eng, 2004; 193: 2719–2743.

[33] Li X, Tang H. A consistent return mapping algorithm for pressure-dependent elastoplastic Cosserat continua and modeling of strain localization. Comput Struct, 2005; 83: 1–10.

[34] Neff P. A finite-strain elastic–plastic Cosserat theory for polycrystals with grain rotations. Int J Eng Science, 2006; 44: 574–594

[35] Sievert R, Forest S, Trostel R. Finite deformation Cosserat-type modeling of dissipative solids and its application to crystal plasticity. J de Physique, 1998; 8: 357–364.

[36] Mori K. Finite element simulation of powder forming and sintering. Comput Meth Appl Mech Eng, 2006; 195: 6737–6749

[37] Khoei AR, Tabarraie AR, Gharehbaghi SA. H-adaptive mesh refinement for shear band localization in elasto-plasticity Cosserat continuum. Comm Nonl Science Numer Simul, 2005; 10: 253-286.

[38] Khoei AR, Gharehbaghi SA, Tabarraie AR, Riahi A. Error estimation, adaptivity and data transfer in enriched plasticity continua to analysis of shear band localization. Appl Math Model, 2006; in press.

[39] Malvern L. Introduction to the Mechanics of a Continuous Medium. Prentice-Hall, 1969.

[40] Simo JC, Taylor RL. Consistent tangent operator for rate independent elasto-plasticity. Comput Meth Appl Mech Eng, 1985; 48: 101–118